Research Article

Ping Ye, Yuanyuan Ye, Xiaojing Chen, Hanbing Zou, Yan Zhou, Xue Zhao, Zhaohua Chang, Baosan Han*, and Xianming Kong*

Ultrasmall Fe_3O_4 nanoparticles induce S-phase arrest and inhibit cancer cells proliferation

https://doi.org/10.1515/ntrev-2020-0006
Received Aug 05, 2019; accepted Aug 20, 2019

Abstract: The ultrasmall nanoparticles easily lead to a more seriously response than larger nanoparticles because of their physicochemical features. It is essential to understand their cytotoxicity effects for their further application. Here, we used ultrasmall 9 nm Fe_3O_4 NPs to explore its cytotoxicity mechanism on breast cancer cells. We demonstrated 9 nm Fe_3O_4 NPs was effectively internalized into cells and located in nucleus, subsequently, it inhibited DNA synthesis through inducing S-phase arrest. Moreover, 9 nm Fe_3O_4 NPs induced ROS production and oxidative damage by disturbing the expression of antioxidant-related genes (HMOX-1, GCLC and GCLM), which resulted in the enhancement of cells apoptosis and inhibition of cell proliferation, suggesting its potential to be used as therapeutic drug.

Keywords: breast cancer, nanoparticles, S-phase arrest, reactive oxygen species, gene expression

***Corresponding Author: Baosan Han:** Department of Breast Surgery, Xinhua Hospital, School of Medicine, Shanghai Jiao Tong University, Shanghai, 200092, China; Email: hanbaosan@126.com
***Corresponding Author: Xianming Kong:** State Key Laboratory of Oncogenes and Related Genes, Shanghai Cancer Institute, Renji Hospital, School of Medicine, Shanghai Jiao Tong University, Shanghai, 200032, China; Xinjiang Tumor Hospital affiliated to Xinjiang Medical University, Xinjiang, 830011, China; Email: kxm666@aliyun.com
Ping Ye, Zhaohua Chang: Shanghai Institute for Minimally Invasive Therapy, School of Medical Instrument and Food Engineering, University of Shanghai for Science and Technology, Shanghai 200093, China
Yuanyuan Ye: Department of Breast Surgery, Xinhua Hospital, School of Medicine, Shanghai Jiao Tong University, Shanghai, 200092, China
Yuanyuan Ye and **Ping Ye** contributed equally to this work
Xiaojing Chen, Hanbing Zou, Yan Zhou, Xue Zhao: State Key Laboratory of Oncogenes and Related Genes, Shanghai Cancer Institute, Renji Hospital, School of Medicine, Shanghai Jiao Tong University, Shanghai, 200032, China

1 Introduction

The nanoparticles exhibit increased application in biomedical fields such as contrast agent, disease detection and drug delivery [1–3], but their interaction with cell remain poorly understood, especially for the ultrasmall nanoparticles. Owing to cells have a diameter range 10 to 100 μm, cellular parts are much smaller, and proteins are even smaller with a typical range of just 5 to 50 nm [4], therefore the smaller the nanoparticles size, the more the interaction with cellular components, which easily induce more toxic effect than larger particles of the same materials because of larger surface area, enhanced chemical reactivity and easier cellular penetration [5–7].

Fe_3O_4 NPs lies in its promising application in these fields of tumor diagnosis and drug delivery due to their physicochemical features, including biocompatibility and magnetic properties [8–10]. Therefore, we used ultrasmall Fe_3O_4 nanoparticles (Fe_3O_4 NPs) with 9 nm size to investigate the interaction mechanism of ultrasmall nanoparticles with MCF-7 breast cancer cell. We discovered that the Fe_3O_4 NPs with 9 nm size, it could inhibit the proliferation through enhancing oxidative stress apoptosis of MCF-7 breast cancer cell and disturbing cell cycle (Figure 1). This research contributes to further illustrate the mechanism of Fe_3O_4 NPs inhibiting MCF-7 breast cancer cells, and suggests the Fe_3O_4 NPs alone have potential as an antitumor drug to kill tumor.

2 Experimental details

2.1 Materials

Fe $(acac)_3$ was purchased from Acros Organics (Geel, Belgium). Fetal bovine serum (FBS), dulbecco modified eagle medium (DMEM), Streptomycin, Trizol reagent and trypan blue were purchased from Thermo Fisher Scientific (Waltham, MA, USA). Cell-Light EdU DNA cell proliferation kit was purchased from Guangzhou Ribo-

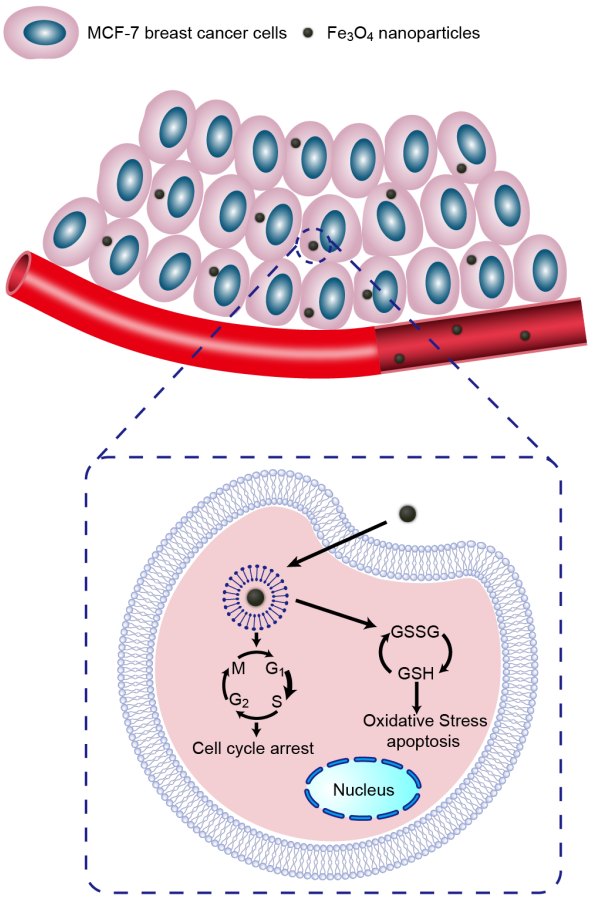

Figure 1: Schematic diagram of interaction of Fe_3O_4 NPs and MCF-7 breast cancer cell

Bio Co., Ltd. (Guangzhou, China). Triethylene glycol, Propidium iodide (PI) and Annexin V/PI apoptosis detection kit were purchased from Sigma-Aldrich China Co., Ltd. (Shanghai, China). Total Glutathione Assay Kit, 2',7'–dichlorofluorescin diacetate (DCFH-DA) and bicinchoninic acid assay kit were purchased from Jiangsu Beyotime Institute of Biotechnology (Haimen, Jiangsu, China), SYBR Premix Ex Taq Perfect Real Time Kit was purchased from Otsu Takara Bio. Inc. (Otsu, Shiga, Japan). Horseradish peroxidase was purchased from Abcam (Cambridge, MA, USA). Other reagents were purchased from Sinopharm Chemial Reagent Co., Ltd. (Shanghai, China).MCF-7 breast cancer cells obtained from the Shanghai Cell Institute Country Cell Bank (Shanghai, China) were cultured in high-glucose DMEM containing 10% fetal bovine serum, 100 U/mL penicillin and 100 ug/mL streptomycin at 37°C in a humidified environment containing 5% CO_2.

2.2 Synthesis and characterization of Fe_3O_4 NPs

9-nanometer Fe_3O_4 NPs were prepared using the polyol method [11]. Briefly, 2 mmoL $Fe(acac)_3$ and 25 mL triethylene glycol was directly added into a three-neck round-bottomed flask equipped with condenser, magnetic stirrer, thermograph, heating mantle and stirred under argon. The mixture was heated to 180°C at a rate of 3°C min^{-1} for maintaining 30 min, then was quickly heated to 280°C for an another 30 min of reflux. After cooling down to room temperature, a black homogeneous colloidal suspension contained of magnetite nanoparticles was obtained. Then, 2 mmoL Fe $(acac)_3$ was again added to react according the aforementioned contidition. The obtained solution was dialysis in distilled water and then was collected with a magnetic to obtain 9 nm Fe_3O_4 NPs. Subsequently, the Fe_3O_4 NPs was characterized using transmission electron microscope (TEM), dynamic light scattering (DLS) and X-ray diffractometer (XRD).

2.3 Cell viability

Cell viability was determined using cell count method [12]. MCF-7 breast cancer cells (4×10^4 cells/well) were seeded in 12-well plate and were cultured for 24 h. Different concentration of Fe_3O_4 NPs with 9 nm particle size were added and were separately incubated for 24 h, 48 h and 72 h. Cells were then harvested and resuspended in 1 mL PBS and were counted manually with 0.4% Trypan blue in a haemocytometer chamber.

2.4 Cell proliferation imaging

Cell proliferation was imaged using EdU cell proliferation imaging kit [13]. Briefly, MCF-7 breast cancer cells (4×10^4 cells/well) were seeded in 96-well plates and were incubated for 24 h. Different concentration of Fe_3O_4 NPs with 9nm particle size were added and were incubated for 48 h. The cells were then treated with 50 mM EdU culture medium for 2 h and washed twice (5 min/once) with PBS, followed by incubation with 4% PFA for 30 min. After removing the solution from the wells, 50 uL glycine (2 mg/mL) was added and were incubated for 5 min. Next, 100 uL PBS solution containing 0.5 % Triton X-100 was added and were incubated for 10 min. Thereafter, 100 uL Apollo® staining reaction liquid was added and were incubated for 30 min. Finally, cells were incubated with 100 u L of Hoechst 33342 for 30 min, washed

three times (5 min/once), and imaged using an IX-51 fluorescence microscope from Olympus Optical Company, Ltd (Tokyo, Japan). Data of cell proliferation was then calculated using Image-Pro Plus 7.0 software from Media Cybemetics, Inc. (Rockville, USA).

2.5 Cell apoptosis

Cell apoptosis was measured using Annexin V/PI apoptosis detection kit. Briefly, MCF-7 cells (1.6×10^5 cells/well) were seeded into 6-well plate and were incubated for 24 h. Different concentration of Fe_3O_4 NPs with 9 nm particle size were added and were incubated for 48 h. Cells were collected and were resuspended in 100 uL of binding buffer at a density of 1×10^6 cells/mL. Subsequently, 5uL annexin V-FITC and 5 uL PI were added and were incubated for 15min. 400uL binding buffer was then added to suspension and were gently mixed. Finally, cells were analyzed through FACSCalibur flow cytometry (BD Biosciences, San Diego, CA, USA).

2.6 Cell cycle

MCF-7 breast cancer cells (1.6×10^5 cells/well) were seeded into 6-well plate and were incubated for 24 h. Different concentrations of Fe_3O_4 NPs with 9 nm particle size was added and incubation for 48 h. Cells was then collected and fixed in 70% ethanol at 4°C overnight. Cells were then resuspended in PBS and were incubated at 37°C in the dark for 30 min in the solution of 10 mg/mL RNase and 1 mg/mL PI. Finally, cells were analyzed using FACSCalibur flow cytometry.

2.7 Intracellular distribution

Intercellular distribution of Fe_3O_4 NPs was evaluated using TEM [13]. MCF-7 breast cancer cells were cultured in 10 cm plate and were incubated for 24 h. Fe_3O_4 NPs with 9 nm particle size was added to the plate and were incubated for 3h, cells were then washed with phosphate buffered saline (PBS) and were fixed in a 0.1 M PBS solution containing 2.5% glutaraldehyde for 30min. Afterward, cells were collected and were washed with PBS, trypsinized, harvested, and resuspended in 500 μL stationary liquid containing 4% paraformaldehyde and 5% glutaraldehyde. Cells were embedded in agar gel and were then cut into 1-mm slices. Each slice was again fixed using osmic acid, dehydrated, embedded, and imaged using TEM.

2.8 GSH analysis

Total intracellular glutathione (GSH) levels were measured using Total Glutathione Assay Kit [14]. Briefly, MCF-7 cells (1.6×10^5cells/well) were seeded into 6-well plate and were incubated for 24 h. Different concentration of Fe_3O_4 NPs with 9 nm particle size were added and were incubated for 48 h. Cells were then washed with PBS, freezed thawing rapidly twice using liquid nitrogen and 37°C water, and were centrifuged at 10,000 × g for 10 min. The supernatant was reacted with DTNB (5,5'-Dithiobis (2-nitrobenzoic acid)) for 5 min at 25°C to obtain the yellow-colored product. Afterwards, the product was assayed at 412 nm absorbance using a microplate reader (Bio-Tek, USA). The GSH concentrations were determined by comparison with standards.

2.9 ROS analysis

Intracellular reactive oxygen species (ROS) levels were assayed using FACSCalibur flow cytometer [14]. Briefly, MCF-7 breast cancer cells (1.6×10^5 cells/well) were seeded into 6-well plate and were incubated for 24 h. Different concentration of Fe_3O_4 NPs with 9 nm particle size were added and were incubated for 48 h. Then, cells were washed with FBS free medium and were incubated with 10 μM DCFH-DA for 30 min at 37°C in the dark. Subsequently, cells were washed twice with FBS free medium to remove the additional dye, and were incubated in FBS free medium for an additional 30 min at 37°C to allow complete de-esterification of intracellular diacetates. Cells were then harvested by trypsinization and at least 2×10^4 cells from each sample were analyzed using flow cytometry.

2.10 qRT-PCR analysis

The mRNA levels of genes involved in oxidative stress (HMOX1, GCLC and GCLM) were measured using quantitative the Applied Biosystems StepOnePlus™Real-Time PCR System (qRT-PCR) (Life Technologies, USA). Briefly, MCF-7 cells (1.6×10^5 cells/well) were seeded into 6-well plate and incubated for 24 h. Different concentration of Fe_3O_4 NPs with 9 nm particle size were added and incubated for 48 h. Cells were lysed with the addition of trizol reagent. RNA was extracted and purified utilizing standard phenol/chloroform extraction procedures. cDNA was obtained using a mixture containing 5 × PrimeScript RT Master Mix (Takara), Total RNA, and RNase Free dH_2O. Subsequently, qRT-PCR analysis was performed using qRT-

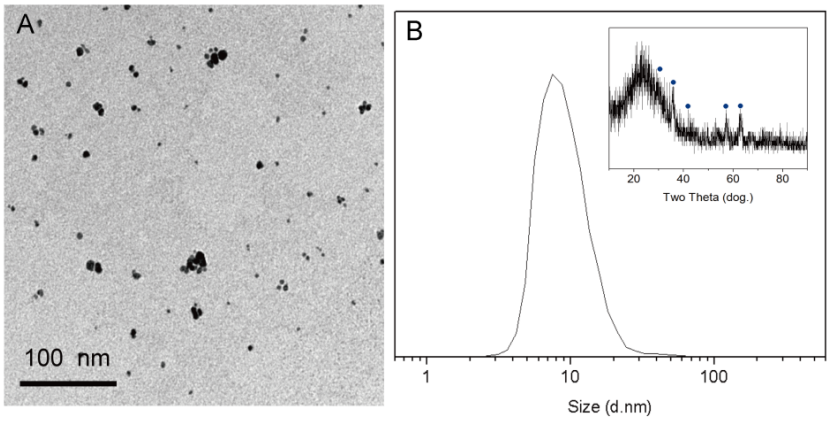

Figure 2: Characterization of nanoparticles: TEM (A) and DLS (B) images of Fe_3O_4 NPs with 9nm particle sizes; the inserted image is the XRD image

PCR with the SYBR Premix Ex Taq Perfect Real Time Kit. The PCR reaction consisted of initial thermal activation at 95°C for 30 s and 40 cycles. Each cycle was as follows: 95°C for 5 s; 60°C for 34 s. PCR products were verified by analysis of melt curves and amplification plots. Quantitative values were acquired from linear regression of the PCR standard curve. The primer sequences of the amplified genes are as follows: HMOX1(Heme oxygenase-1), forward 5'-TGGAGACTCCCAGAGGGAAG-3' and reverse 5'-CACCGGACAAAGTTCATGGC-3'; GAPDH, forward 5'-GGATGCAGAAGGAGATCACTG-3' and reverse 5'-CGATCCACACGGAGTACTTG-3', GCLC(glutamate-cysteine ligase, catalytic subunit), forward 5'-TGCACAATAACTTCATTTCCCAGT-3' and reverse 5'-ATCCGGCTTAGAAGCCCTTG-3', GCLM(glutamate-cysteine ligase, modifier subunit), forward 5'-GGTCAGGGAGTTTCCAGATGT-3' and reverse 5'-CTGTGCAACTCCAAGGACTGA-3'.

2.11 Western Blotting

MCF-7 cells (1.6×10^5 cells/well) were seeded into 6-well plate and were incubated for 24 h. Different concentration of Fe_3O_4 NPs with 9nm particles size were added and incubated for 48 h. Cells were lysed and denatured, and the total protein concentration of cell extracts was determined using the bicinchoninic acid assay kit with BSA as a standard. Equal quantities (80 μg protein per lane) of total proteins were separated by SDS-PAGE (10%, 12% gels) under reducing conditions. The proteins were then electrophoretically transferred to nitrocellulose membranes. The membranes were blocked with 5% skimmed milk and incubated with anti-hmo × 1, anti-gclc, anti-gclmand anti-gapdh antibodies, respectively (1:1000; Cell Signaling Technology) at 4°C overnight. This was followed by an incubation with goat anti-rabbit/anti-mouse secondary antibody conjugated with horseradish peroxidase (1:5000). An equal loading of each lane was evaluated by immunoblotting the same membranes with β-actin antibody after the detachment of previous primary antibody. Photographs were taken and the optical densities of bands were scanned and quantified with Gel Doc 2000 (BioRad, USA).

2.12 Statistics

Data were presented as mean ± standard deviation (S.D.) of at least three independent experiments. The significance of differences in data of different groups were appropriately determined by the unpaired Student's *t*-test at $P<0.05$.

3 Results and discussion

3.1 Characterization of Fe_3O_4 NPs

In order to research the relative mechanism of toxicity of ultrasmall Fe_3O_4 NPs in MCF-7 cells, we synthesis the Fe_3O_4 NPs using the polyol method. XRD result suggest that the observed diffraction pattern can be indexed to Fe_3O_4 (JCPDS file 19-0629), demonstrating the Fe_3O_4 nanoparticles are successfully synthesized. TEM and DLS results verify that Fe_3O_4 NPs exhibit a spherical morphology and a diameter of 9 nm, and they have uniform and good size distribution (Figure 2A,2B).

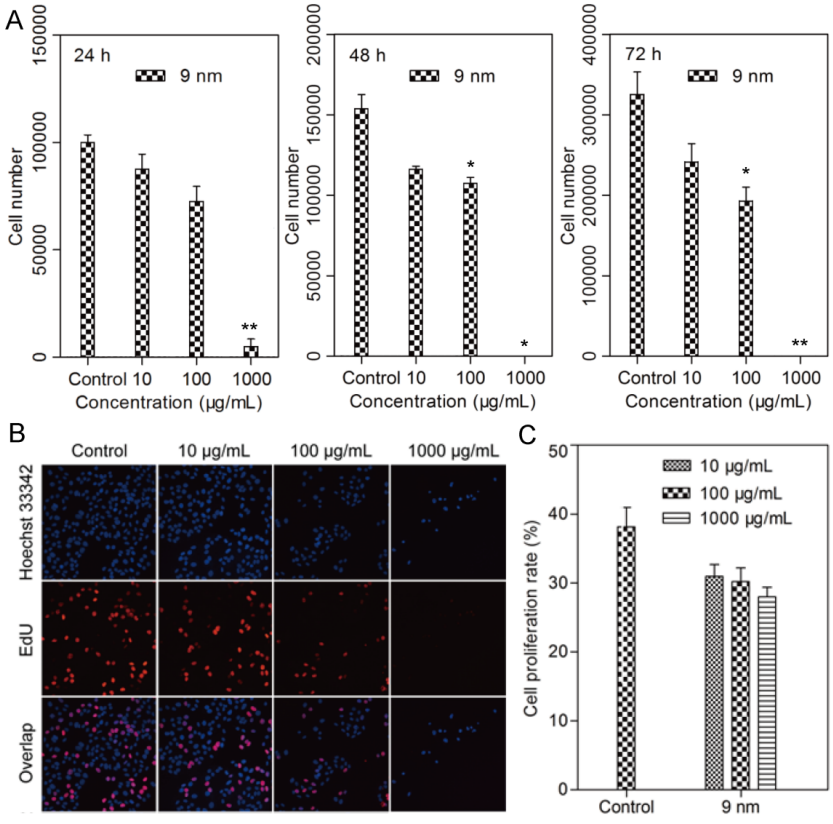

Figure 3: The influence of nanoparticles on cell proliferation: (A) Cell growth number of Fe_3O_4 NPs-treated MCF-7 cells. (B) The proliferation image of MCF-7 cells treated with Fe_3O_4 NPs for 48h. Blue fluorescence is from Hoechst 33342 nuclear staining. Red fluorescence is from Apollo DNA staining labelled by EdU. (C) Data quantitative image of cell proliferation. Data are presented as mean ±S.D. (n=3)

3.2 Cell viability and cell proliferation imaging

Cell count method was employed to evaluate the effect of 9 nm Fe_3O_4 NPs for cell growth viability. As shown in Figure 3A, cell growth number gradually increased with the extension of incubation time from 24h to 72h in the control group alone. As the increase of Fe_3O_4 NPs incubation concentration from 10 μg/mL to 1000 μg/mL, cell growth number exhibited a concentration-dependent decrease. Especially at 1000 μg/mL incubation concentration, it reduced the cells number to the minimum, demonstrating that the Fe_3O_4 NPs affect the cells number in a concentration-dependent manner.

Cell proliferation depends on both cell division and cell death [15]. EdU cell proliferation imaging was carried out to further illustrate the influence mechanism of Fe_3O_4 NPs for cell proliferation. Edu easily inserted to DNA in the course of DNA synthesis, it thereby is employed to label S-phase cells for monitoring DNA synthesis and trace of the EdU-labelled cells when they progressed through the cell cycle and divided. As indicated in overlap image of Figure 3B, a gradually diminishing red fluorescence in quantify were observed in MCF-7 cells exposed to an increasing Fe_3O_4 NPs concentration from 10 μg/mL to 1000 μg/mL, demonstrating that Fe_3O_4 NPs disturb DNA synthesis of MCF-7 cells in a concentration-dependent manner and thereby further decrease cell proliferation (Figure 3C), which is consistent with the result of cell growth number. Especially for the high concentration of Fe_3O_4 NPs, it exhibited the most obvious interference efficiency. These experimental results suggested that the difference in concentration of nanoparticles induces different toxicity response.

3.3 Cell apoptosis

Cell apoptosis assay was performed to illustrate the mechanisms of Fe_3O_4 NPs affecting MCF-7 cells growth and proliferation, in which two different concentrations of Fe_3O_4 NPs was employed. As shown in Figure 4A and 4B, compared with control group, 15 μg/mL Fe_3O_4 NPs-treated cells exhibited no less low survival rates, and the early and

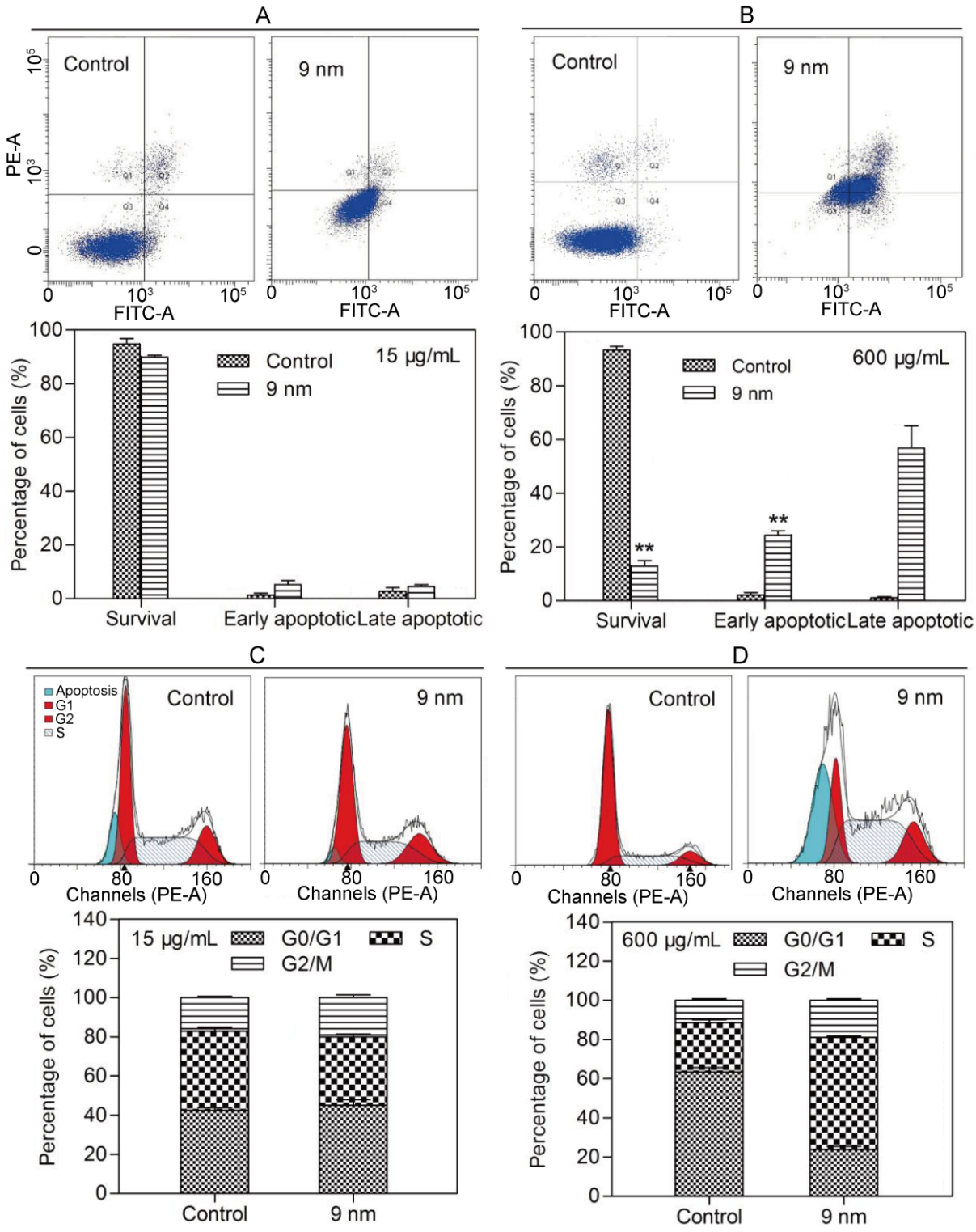

Figure 4: The analysis of cell apoptosis and cell cycle: Flow cytometer analysis on cell apoptosis of MCF-7 cells incubated with 9 nm Fe_3O_4 NPs for 48 h at a concentration of 15 μg/mL (A) and 600 μg/mL (B). Flow cytometer analysis on cell cycle of MCF-7 cells with 9 nm Fe_3O_4 NPs for 48 h at a concentration of 15 μg/mL (C) and 600 μg/mL (D). All histograms are quantitative figures for the corresponding cycle and apoptosis. Data are presented as mean ± S.D. (n=3)

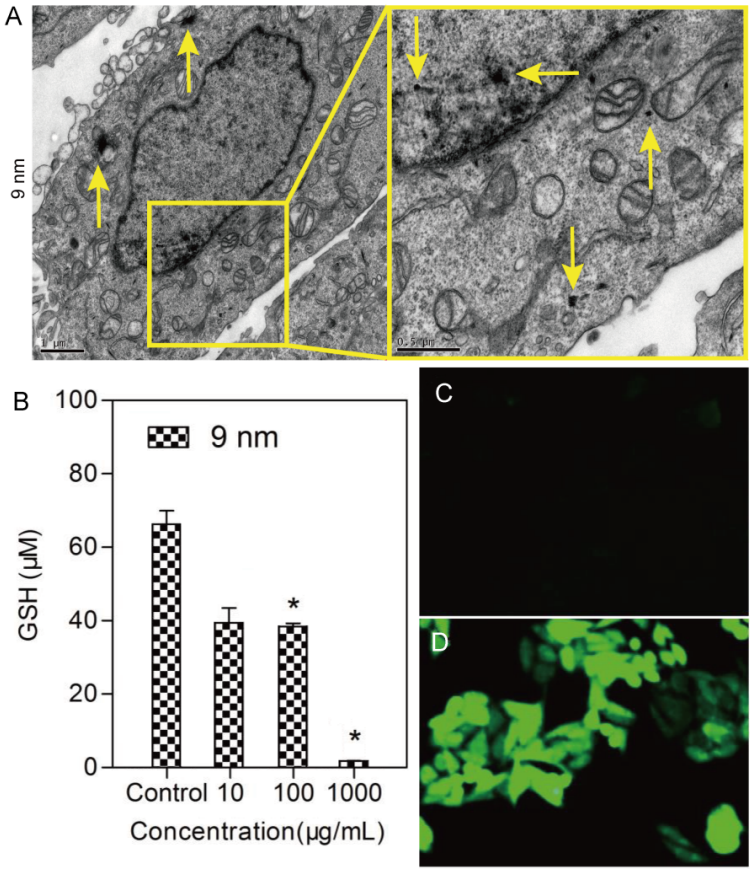

Figure 5: The production of GSH and ROS induced by nanoparticles: (A) Intracellular distribution image of Fe_3O_4 NPs in cells exposed to Fe_3O_4 NPs (600 μg/mL) for 3 h. The corresponding image (right) is the magnified image of regional image in A figure. (B) GSH level of cells treated with Fe_3O_4 NPs for 48h. The ROS images of cells treated separately with control (C) and 9 nm Fe_3O_4 NPs (D) for 48h. Data are presented as mean ± S.D. (n=3)

late apoptosis of cells treated with 15 μg/mL Fe_3O_4 NPs also were no obviously variation, suggesting a negligible influence of Fe_3O_4 NPs for cell apoptosis at the incubation concentration of 15 μg/mL.

However, as the concentration increasing to 600 μg/mL, the survival rate of cells treated with Fe_3O_4 NPs obviously decreased as compared to the control. The early apoptosis of cells treated with Fe_3O_4 NPs approximated 30%, which were obviously upregulated as compared to the control. For the late apoptosis, Fe_3O_4 NPs-treated cells was upregulated significantly to 60% as compared to the control, indicating that concentration of Fe_3O_4 NPs obviously affect cell apoptosis, which predominantly result from disturbing the early and late apoptosis of cells.

3.4 Cell cycle

Cell cycle involves DNA replication and cell separation, consisting of four distinct phases: G1 phase, S phase, G2 phase and M phase. The cell cycle deregulation can induce cell apoptosis [16–18]. We carried out this experiment to illustrate the mechanism of Fe_3O_4 NPs interfering cell cycle. As can be seen from Figure 4C and 4D, G2/M, S and G0/G1 of cells exposed to Fe_3O_4 NPs with the concentration of μg/mL were regular and were no obviously change as compared to the control, cell cycle phase can be ranked in increasing order: G2/M>S>G0/G1. As the concentration increasing to 600 μg/mL, the cycle of cells exposed to Fe_3O_4 NPs was disrupted, about 60% and 20% of cell population were separately at S and G0/G1 phase, a primarily S-phase cell-cycle arrest was confirmed. For further exploring the mechanism of S-phase cell-cycle arrest, we performed the intracellular distribution experiment of Fe_3O_4 NPs. As shown in Figure 5A, Fe_3O_4 NPs with the concentration of 600 μg/mL internalized by cells mostly distributed in autophagosome and nuclear of cells. Whereas the nanoparticles in the cell nucleus could affect the DNA synthesis, and potentially induced apoptosis, thereby decreased cell proliferation accordingly.

3.5 Intracellular glutathione and ROS production

Glutathione (GSH) represents the major intracellular redox buffer in cells, it is the first line of cellular defense mechanism against oxidative injury when nanoparticles was internalized by cells [19–21]. The experimental results were shown in Figure 5B, Fe_3O_4 NPs induced a dose-dependent decrease of GSH concentration in MCF-7 cells as compared to the control alone. Especially at the concentration of 1000 μg/mL, the GSH level of cells treated with Fe_3O_4 NPs significantly decreased to about 5 μM, which induced a reduced by 92% compared to control.

Owing to ROS generation could directly cause oxidative injury and play an important role in cell signaling and regulate inflammatory responses, toxicity of drugs, apoptosis or programmed cell death [22, 23], we then assayed the expressed level of reactive oxygen species (ROS). As can be seen from Figure 5C and 5D, compared with the control, a high green fluorescence intensity was observed in cells treated with Fe_3O_4 NPs with the concentration of 1000 μg/mL, demonstrating that Fe_3O_4 NPs induce higher ROS production in MCF-7 cells, In combination with the experimental result of GSH, it can be concluded that the low GSH level induce high ROS expression, and thus result in the oxidative damage and cause cell apoptosis.

3.6 Expression of anti-oxidative genes and proteins

To further investigate the mechanism of Fe_3O_4 NPs inducing oxidative response in MCF-7 cells, the mRNA expressions of three antioxidant-related genes (HMOX-1, GCLC and GCLM) and their protein levels were measured [24]. We found that the expressions of HMOX-1 mRNA, GCLC mRNA, and GCLM mRNA in cells with treated Fe_3O_4 NPs were upregulated when compared with the control, moreover, a gradually increasing trend was observed with the incubation concentration enhancing from 10 to 500 μg/mL (Figure 6A). When the incubated concentration ranges from 500 μg/mL to 1000 μg/mL, the expression of HMOX-1 mRNA, GCLC mRNA, and GCLM mRNA in cells treated with Fe_3O_4 NPs declined, suggesting that the difference of the concentration induce the different toxicity response.

The expressions of HMOX-1, GCLC, and GCLM protein were then determined using western blotting (Figure 6B). The HMOX-1 protein expression level in cells treated with Fe_3O_4 NPs was weaker than the GCLC and GCLM protein expression level at the incubation concentration from 0 to 100μg/mL, suggesting that the Fe_3O_4 NPs induce an oxidative damage that is mainly mediated by disturbing the protein expressions of GCLC and GCLM. However, we also noticed that the expressions of HMOX-1, GCLC and GCLM protein exhibited a minimum expression at the incubated concentration of 1000 μg/mL, which was attributed to a low protein synthesis caused by a high oxidative damage and contributed to induce an effective inhibition for MCF-7 cell growth.

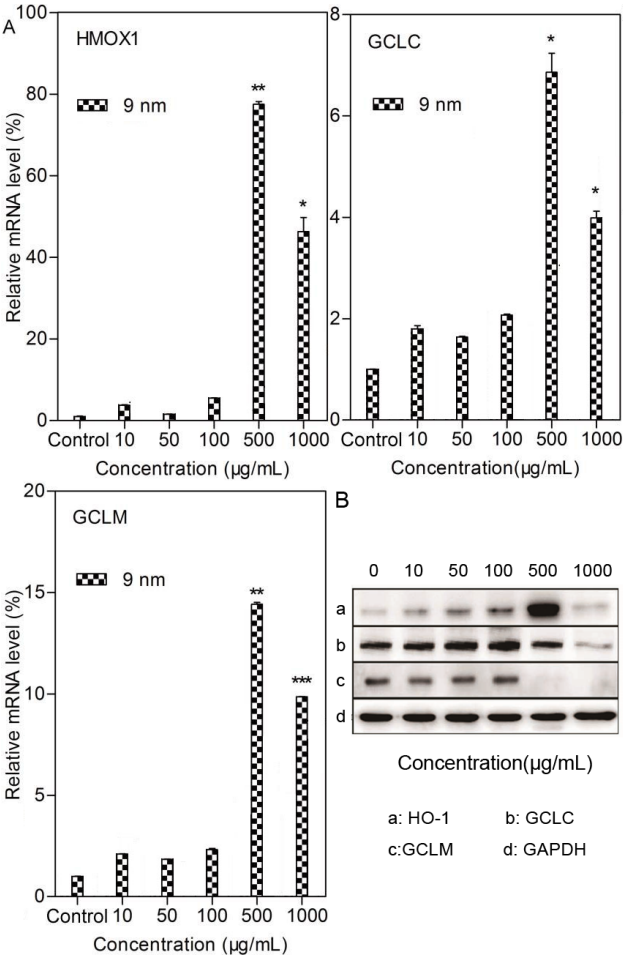

Figure 6: The expression of anti-oxidative genes and proteins induced by nanoparticles: (A) The expression levels of the HMOX-1, GCLC, and GCLM mRNA in MCF-7 cells treated with 10 μg/mL, 50 μg/mL, 100 μg/mL, 500 μg/mL and 1000 μg/mL Fe_3O_4 NPs 9 nm particle size for 48 h. (B) The expression of anti-oxidative related proteins in MCF-7 cells treated with 10 μg/mL, 50 μg/mL, 100 μg/mL, 500 μg/mL and 1000 μg/mL Fe_3O_4 NPs with 9 nm particle size for 48 h. Data were presented as mean ± S.D. (n=3)

4 Conclusions

In summary, we demonstrated the ultrasmall 9nm Fe_3O_4 NPs effectively inhibited DNA synthesis and enhanced cell

apoptosis by inducing S-phase arrest, which thereby reduced the cell growth and proliferation. In addition, 9nm Fe_3O_4 NPs remarkably disturbed the expressions of HMOX-1 mRNA, GCLC mRNA, and GCLM mRNA, inducing the high ROS production and decreased GSH, leading to a seriously oxidative damage for MCF-7 cells, which make 9 nm Fe_3O_4 NPs inhibit the growth of MCF-7 cells. These results suggesting 9 nm Fe_3O_4 NPs have potential to be used as the antitumor drug.

Conflict of Interests: The authors declare no conflict of interest regarding the publishing of this paper.

Acknowledgement: This work was founded by the National Natural Science Foundation of China (No.81771968, No.81472842 and No.81560495) and the China Postdoctoral Science Foundation (2017M611589).

References

[1] Baetke S.C., Lammers T., Kiessling F., Applications of nanoparticles for diagnosis and therapy of cancer, Br. J. Radiol., 2015, 88(1054), 20150207.

[2] Wu T., Ding X., Su B., Soodeen-Lalloo A.K., Zhang L., Shi J.Y., Magnetic resonance imaging of tumor angiogenesis using dual-targeting RGD10-NGR9 ultrasmall superparamagnetic iron oxide nanoparticles, Clin. Transl. Oncol., 2018, 20(5), 599-606.

[3] Das M., Mishra D., Dhak P., Gupta S., Maiti T.K., Basak A., Pramanik P., Biofunctionalized, phosphonate-grafted, ultrasmall iron oxide nanoparticles for combined targeted cancer therapy and multimodal imaging, Small, 2009, 5(24), 2883-2893.

[4] Valdiglesias V., Kilic G., Costa C., Fernandez-Bertolez N., Pasaro E., Teixeira J.P., Laffon B., Effects of iron oxide nanoparticles: cytotoxicity, genotoxicity, developmental toxicity, and neurotoxicity, Environ. Mol. Mutagen., 2015, 56(2), 125-148.

[5] Bakand S., Hayes A., Dechsakulthorn F., Nanoparticles: a review of particle toxicology following inhalation exposure, Inhal. Toxicol., 2012, 24(2), 125-135.

[6] Lee K.J., Browning L.M., Nallathamby P.D., Desai T., Cherukuri P.K., Xu X.H., In vivo quantitative study of sized-dependent transport and toxicity of single silver nanoparticles using zebrafish embryos, Chem. Res. Toxicol., 2012, 25(5), 1029-1046.

[7] British Journal of PharmacologyMedina C., Santos-Martinez M.J., Radomski A., Corrigan O.I., Radomski M.W., Nanoparticles: pharmacological and toxicological significance, Br. J. Pharmacol., 2007, 150(5), 552-558.

[8] Patsula V., Kosinova L., Lovric M., Ferhatovic Hamzic L., Rabyk M., Konefal R., Paruzel A., Slouf M., Herynek V., Gajovic S., Horak D., Superparamagnetic Fe3O4 Nanoparticles: Synthesis by Thermal Decomposition of Iron(III) Glucuronate and Application in Magnetic Resonance Imaging, ACS Appl Mater Interfaces, 2016, 8(11), 7238-7247.

[9] Diana C., Marisa F., Félix C., Eduarda F., Iron Oxide Nanoparticles: An Insight into their Biomedical Applications, Curr. Med. Chem., 2015, 22(15), 1808-1828.

[10] Sato A., Itcho N., Ishiguro H., Okamoto D., Kobayashi N., Kawai K., Kasai H., Kurioka D., Uemura H., Kubota Y., Watanabe M., Magnetic nanoparticles of Fe3O4 enhance docetaxel-induced prostate cancer cell death, Int. J. Nanomed., 2013, 8, 3151-3160.

[11] Cai W., Wan J., Facile synthesis of superparamagnetic magnetite nanoparticles in liquid polyols, J. Colloid Interface Sci., 2007, 305(2), 366-370.

[12] Kim J.A., Aberg C., Salvati A., Dawson K.A., Role of cell cycle on the cellular uptake and dilution of nanoparticles in a cell population, Nature Nanotech., 2012, 7(1), 62-68.

[13] Liu P., Sun Y., Wang Q., Sun Y., Li H., Duan Y., Intracellular trafficking and cellular uptake mechanism of mPEG-PLGA-PLL and mPEG-PLGA-PLL-Gal nanoparticles for targeted delivery to hepatomas, Biomaterials, 2014, 35(2), 760-770.

[14] Xie Y., Liu D., Cai C., Chen X., Zhou Y., Wu L., Sun Y., Dai H., Kong X., Liu P., Size-dependent cytotoxicity of Fe3O4 nanoparticles induced by biphasic regulation of oxidative stress in different human hepatoma cells, Int. J. Nanomed., 2016, 11, 3557-3570.

[15] Yue Y., Behra R., Sigg L., Schirmer K., Silver nanoparticles inhibit fish gill cell proliferation in protein-free culture medium, Nanotoxicology, 2016, 10(8), 1075-1083.

[16] Viallard J.F., Lacombe F., Belloc F., Pellegrin J.L., Reiffers J., [Molecular mechanisms controlling the cell cycle: fundamental aspects and implications for oncology], Cancer Radiother., 2001, 5(2), 109-129.

[17] Wagner H.P., Cell cycle control and cancer, Indian J. Pediatr., 1998, 65(6), 805-814.

[18] Hu Z., Holzschuh J., Driever W., Loss of DDB1 Leads to Transcriptional p53 Pathway Activation in Proliferating Cells, Cell Cycle Deregulation, and Apoptosis in Zebrafish Embryos, PLoS One, 2015, 10(7), e0134299.

[19] Diaz Vivancos P., Wolff T., Markovic J., Pallardo F.V., Foyer C.H., A nuclear glutathione cycle within the cell cycle, Biochem. J., 2010, 431(2), 169-178.

[20] Rahman Q., Abidi P., Afaq F., Schiffmann D., Mossman B.T., Kamp D.W., Athar M., Glutathione redox system in oxidative lung injury, Crit. Rev. Toxicol., 1999, 29(6), 543-568.

[21] Shan X.Q., Aw T.Y., Jones D.P., Glutathione-dependent protection against oxidative injury, Pharmacol. Ther., 1990, 47(1), 61-71.

[22] Biochemical PharmacologyGloire G., Legrand-Poels S., Piette J., NF-kappaB activation by reactive oxygen species: fifteen years later, Biochem. Pharmacol., 2006, 72(11), 1493-1505.

[23] Lander H.M., An essential role for free radicals and derived species in signal transduction, FASEB J., 1997, 11(2), 118-124.

[24] Vaz M., Machireddy N., Irving A., Potteti H.R., Chevalier K., Kalvakolanu D., Reddy S.P., Oxidant-induced cell death and Nrf2-dependent antioxidative response are controlled by Fra-1/AP-1, Mol. Cell. Biol., 2012, 32(9), 1694-1709.